Spatial and Temporal Characteristics of Propagating Deformation Bands in AA5182 Alloy at Room Temperature

R. NOGUEIRA DE CODES, O.S. HOPPERSTAD, O. ENGLER, O.-G. LADEMO, J.D. EMBURY, and A. BENALLAL

The spatial and temporal characteristics of propagating deformation bands in the Al-Mg alloy AA5182 in O temper were studied experimentally at room temperature. Tensile tests were carried out on flat specimens at strain rates in the range from 10^{-5} to 10^{-1} s^{-1}. Digital image correlation (DIC) and digital infrared thermography (DIT) were applied to monitor the propagating bands. It was found that the material exhibits a sharp yield point, and Lüders bands were seen at all the strain rates. Jerky flow took place all along the Lüders plateau. It thus seems that the Portevin–Le Chatelier (PLC) effect starts at incipient yielding and that there is no critical strain. At the end of the Lüders plateau, PLC bands immediately started to propagate back and forth along the gage section of the specimen. The work hardening of the material decreased consistently with increasing strain rate, while the flow stress on the Lüders plateau was rather unaffected by the strain rate. This indicates that the dynamic strain aging (DSA) mainly affects the strength of the interaction between mobile and forest dislocations. The strain to necking was found to decrease gradually with strain rate for this alloy, which is consistent with the lower work-hardening rate at the higher strain rates.

DOI: 10.1007/s11661-011-0749-1

I. INTRODUCTION

ALUMINUM alloys are important technological materials primarily due to their attractive strength-to-weight ratio. They are used in diverse applications ranging from packaging to the aeronautical industry. Important candidates for such applications are the alloys from the 5000 series whose primary alloying element is Mg. They may be rolled into thin sheets and offer significant strength. However, their plastic deformation at room temperature is discontinuous, with the strain localizing in narrow bands that leave undesirable traces on the surface of the final product. This is the signature of the Portevin–Le Chatelier (PLC) phenomenon, which manifests itself in certain ranges of temperature and strain rate. The repeated strain localization is due to the negative strain rate sensitivity (SRS) of the material, which, in turn, is correlated with smaller scale phenomena associated with interactions between solute and dislocations, referred to as dynamic strain aging (DSA). The technological goal is to increase the SRS to positive values in the range of temperatures and strain rates relevant for industrial processes. This would ensure material stability during processing and would eliminate the PLC phenomenon. In particular, in Al-Mg alloys, it is desirable to increase the SRS and to eliminate the PLC effect at room temperature.

As proposed by Cottrell,[1,2] the unstable plastic flow observed in Al-Mg alloys can be a result of solute-dislocation interaction at the microscopic level. To date, a full understanding of the micromechanical mechanisms and the relevant factors affecting the macroscopic behavior of serrated plastic flow is still lacking. However, the cause of the PLC effect is negative steady-state SRS, which is attributed to DSA associated with conditions when point defects can diffuse toward mobile dislocations and temporarily arrest them.[3,4] The results of DSA are higher flow stress and greater work hardening at lower strain rates than for higher ones, and further serrated stress-strain curves, discontinuous plastic flow, and propagating deformation bands during plastic straining. An interesting historical presentation of the various studies of the PLC effect can be found in Reference 5.

In this article, we provide experimental data on the mechanical behavior of one of the most important commercial alloys from the 5000 series, namely, AA5182 in O temper. Using DIC and DIT, the spatiotemporal characteristics of the Lüders and PLC bands are revealed in tensile tests at different strain rates. This combined use of DIC and DIT enabled us to study the similarities and differences between the two types of localized deformation and the correlation between the strain and temperature increments induced by the deformation band. The experimental observations are

R. NOGUEIRA DE CODES, Associate Professor, is with LMT-Cachan, ENS de Cachan/CNRS/UPMC, F-94235 Cachan, France. O.S. HOPPERSTAD and O.-G. LADEMO, Professors, are with the Structural Impact Laboratory-SIMLab, Centre for Research-Based Innovation (CRI), and Department of Structural Engineering, NTNU, NO-7491 Trondheim, Norway. O. ENGLER, Professor, is with Hydro Aluminium Deutschland GmbH, R&D Center Bonn, D-53014 Bonn, Germany. J.D. EMBURY, Emeritus Professor, is with Material Sciences and Engineering, McMaster University, Hamilton, ON, Canada L8S 4L7. A. BENALLAL, Professor, is with LMT-Cachan, ENS de Cachan/CNRS/UPMC. Contact e-mail: benallal@lmt.ens-cachan.fr

Manuscript submitted August 4, 2010.
Article published online June 22, 2011

discussed in relation to existing models to enhance the understanding of the underlying mechanisms responsible for Lüders and PLC bands.

II. EXPERIMENTAL

Sheets from the alloy AA5182 were produced by conventional DC casting, hot and cold rolling to final gage 1.0 mm, and finally soft annealed (O temper). The chemical composition (wt pct) of the alloy is Si (0.11 pct), Fe (0.21 pct), Cu (0.0215 pct), Mn (0.27 pct), Mg (4.55 pct), Cr (0.0033 pct), Zn (0.005 pct), Ti (0.01 pct), and Al (balance). Figure 1 shows the grain structure of the material in the soft state (longitudinal section). The material exhibited a fine-grained recrystallized microstructure with a characteristic grain size of 11 μm.

Five tests denoted P1, P2, P3, P4, and P5 were carried out to observe and characterize the discontinuous plastic flow and the propagating deformation bands at different overall strain rates. All tests were carried out on the same specimen geometry depicted in Figure 2. It is a flat and smooth specimen with 20-mm width and 100-mm gage length. The specimens were all cut from the rolled sheet and their axial loading direction aligned with the rolling direction. The test program is summarized in Table I The table presents the measured specimen dimensions, applied displacement and strain rates, time to rupture of the specimen, and dimensions of the optical gage. The optical gage defines the square area over which strains are measured with DIC at different locations along the gage length of the specimen. The location then refers to the center of the optical gage.

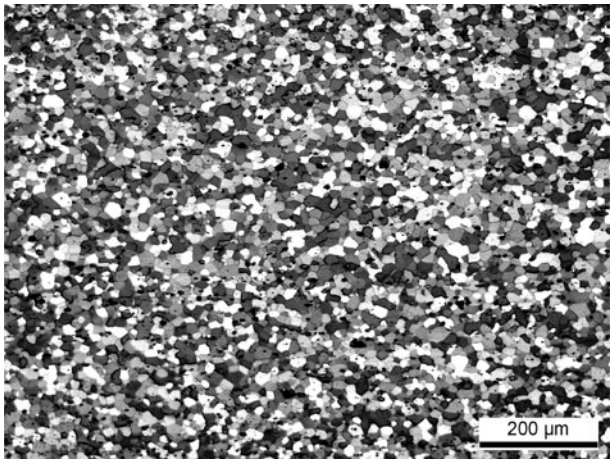

Fig. 1—Microstructure of aluminum alloy AA5182.

The tests were carried out at room temperature in a servohydraulic material testing system (MTS model 810, MTS, Minneapolis, MN) with a 10-kN load cell, in displacement control with crosshead velocity adjusted to the desired nominal strain rate in the range from 10^{-5} to 10^{-1} s^{-1}. Note that all specimens were gripped and clamped at exactly the same positions. The acquisition frequency for the force and displacement was as follows in the five tests: 10 Hz in P1, 50 Hz in P2, 100 Hz in P3 and P4, and 1000 Hz in P5.

Two different techniques were used to observe and eventually characterize the discontinuous plastic flow and the deformation bands spatially and temporally, namely, DIC and DIT. The gage length of the flat specimen was entirely imaged with a fast CCD camera (Photron Ultima APX-RS, Photron USA, Inc., San Diego, CA) on one side and with an infrared camera (JADE 570M, Electrophysics, Sofradir EC, Inc., Fairfield, NJ) on the other side. The imaged zones for DIC and DIT are shown in Figure 2. Prior to the tests, one side of the specimen was decorated with finely sprayed black and white paints to enhance the image contrast for the DIC, while the other was decorated with a fully black paint in order to enhance its emissivity for the

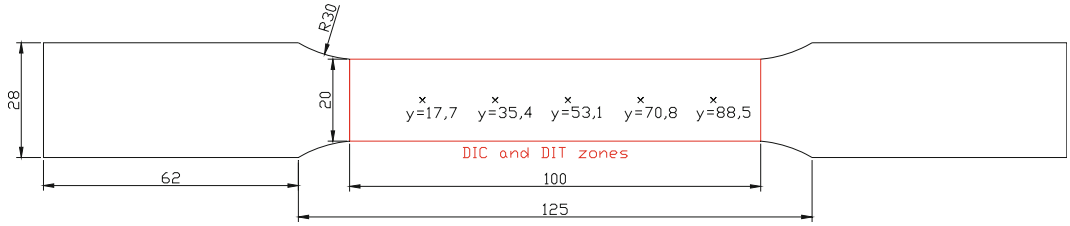

Fig. 2—Specimen geometry in millimeters. The zones monitored with DIC and DIT are shown, as well as locations and coordinates of points where experimental results are described.

Table I. Tensile Test Program

Test	Specimen Dimensions		Crosshead Velocity (mm/s)	Nominal Strain Rate (s^{-1})	Time to Rupture (s)	Optical Gage Dimensions (mm × mm)
	Width (mm)	Thickness (mm)				
P1	19.79	1.03	0.00917	7×10^{-5}	3539.95	10.11 × 10.11
P2	19.74	1.04	0.0436	3.33×10^{-4}	739.36	10.11 × 10.11
P3	19.84	1.01	0.3668	2.8×10^{-3}	81.63	10.11 × 10.11
P4	19.78	1.01	1.31	1×10^{-2}	21.11	10.11 × 10.11
P5	19.72	1.03	13.1	1×10^{-1}	2.679	10.11 × 10.11

Table II. Image Sizes and Acquisition Speeds for Field Measurements Using DIC and DIT

Test	CCD Camera			Infrared Camera		
	Image Size (Pixels)	Acquisition Shutter (Frames/s)	Conversion Factor (mm/Pixel)	Image Size (Pixels)	Acquisition Shutter (Frames/s)	Conversion Factor (mm/Pixel)
P1	128 × 656	50*	0.17360	44 × 239	30**	0.44977
P2	128 × 656	50†	0.17316	47 × 240	25†	0.42
P3	128 × 656	125	0.17404	47 × 239	150	0.42213
P4	128 × 656	125	0.17351	47 × 239	150	0.42085
P5	128 × 656	125	0.17298	46 × 239	150	0.42870

*DIC recorded between 1200 and 1440 s.
**DIT recorded between 1200 and 1500 s.
†DIC and DIT recorded between 0 and 480 s.

DIT. The realization of the texture for DIC is as follows: a first layer of paint is spread, black (or, respectively, white) on which microdroplets of white paint (or black, respectively) are deposited so that the distribution is homogeneous. The texture of the specimen should be heterogeneous, but the distribution of the paint should be as homogeneous as possible. Note that the quality of the speckle pattern is defined by its smoothness. Errors were estimated for both measures. The thermal resolution of the infrared camera used in this work is less than 20 mK. For DIC, an estimate of errors in strain is done by the software Correli^{LMT} (LMT-Cachan, Cachan, France) and was found to be around 6×10^{-3} for the five tests.

For the DIC, the recorded digital images had a 128 × 656 pixel size (Table II). Images were recorded at a shutter speed of 50 or 125 frames per second. The principle of DIC is based on the fact that the distribution of gray scale values of a rectangular area in the initial image corresponds to the distribution of gray scale values of the same area in the destination image. A cumulative strain map can be obtained by comparing each current deformation image with the initial image, while an incremental strain map can be computed by comparing the image at the current load step with the previous image. These maps are computed from the recorded data by the software Correli^{LMT} developed by Hild and co-workers[6,7] Using DIT, the temperature field over the gage area of the specimen is obtained during deformation. The image sizes and acquisition speeds for DIT are also given in Table II.

III. RESULTS

Figure 3 shows the force-displacement curves for all five tests up to failure. While there is no significant influence of strain rate on the yield stress, the work hardening and, thus, the flow stress are found to decrease as the strain rate increases. It is further seen that the ductility (or, more specifically, elongation to necking) decreases when the overall strain rate increases. Very slight necking is observed in all tests, and all specimens failed by through-thickness shear.

Jerky flow is apparent in the force-displacement curves from all the tests. The amplitude of the serrations is seen to increase with increasing strain and to decrease

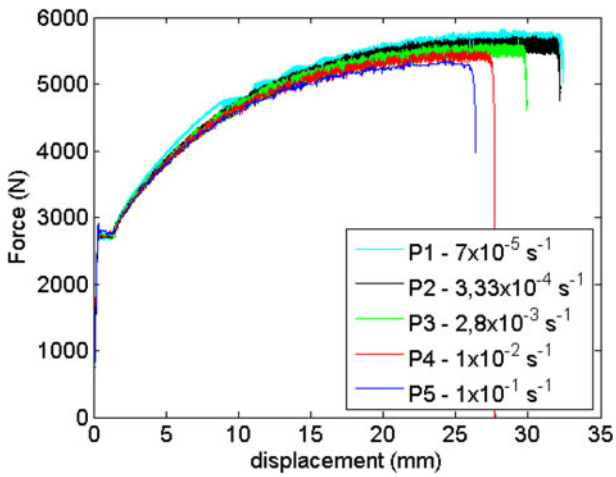

Fig. 3—Load-displacement curves for tests P1, P2, P3, P4, and P5.

with increasing strain rate. All the load-displacement curves display a yield point usually characteristic of the development and growth of a Lüders band. The Lüders plateaus from all tests are shown in Figure 4, where the stress-time curve from the initial phase of the test is plotted. The behavior in the plateau region is compared for the five tests in Figure 5, where the time is normalized with the duration t_p of the Lüders plateau associated with each test. It can be seen that the yield point and the average plateau stress seem to depend only slightly on the strain rate within the actual range. Serrations are observed immediately after the yield point and the characteristics of these serrations are like those of the PLC phenomenon in the sense that their amplitude decreases when the strain rate is increased.

Figure 6 shows the strain-time histories for tests P2, P3, P4, and P5 within the region of the Lüders band, as measured by DIC at the locations depicted in Figure 2 along the longitudinal axis of the specimen (for test P1, there is no DIC and DIT data in the beginning of the test when the Lüders band propagates). These locations correspond to coordinates along this axis, namely, γ equal to 17.7, 35.4, 53.1, 70.8, and 88.5 mm. The strains are measured by optical strain gages located at these positions. The size of these gages is given in Table I. The digital images were processed with the Correli^{LMT} software[6,7] to obtain the corresponding strain history

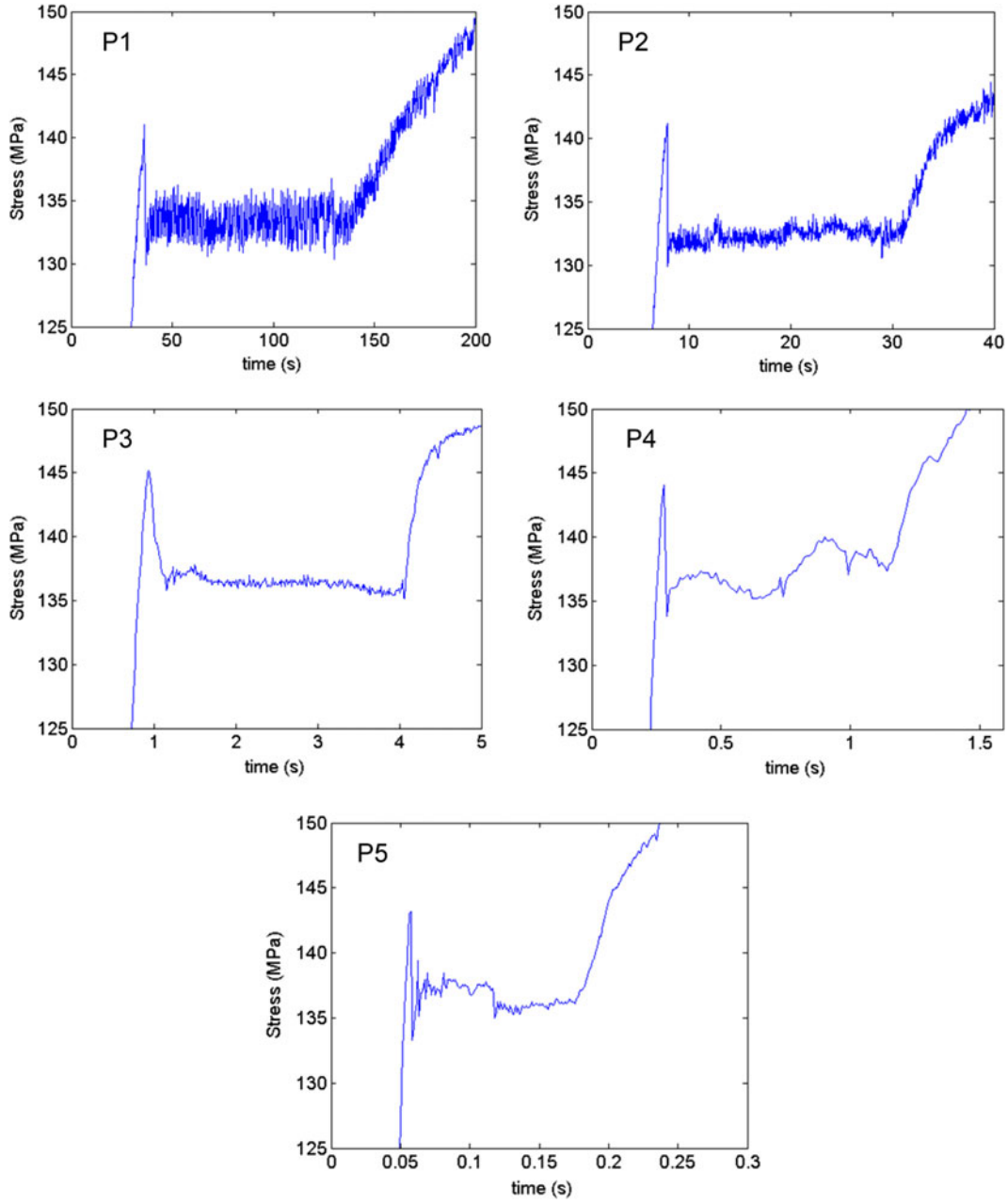

Fig. 4—Stress-time curves from the beginning of tests P1, P2, P3, P4, and P5, showing the yield point and the Lüders plateau.

in these areas. It is seen that at all coordinates the strain increases in the elastic domain and then is nearly constant until the Lüders band passes by the location of the optical gage. At this point, the strain increases rapidly to about 0.010 to 0.015 and then stays nearly constant until the Lüders band has strained the entire gage region of the specimen. From Figure 6, for test P2, it is seen that the Lüders band continuously moves across the specimen, arriving first at $y = 17.7$ mm, then at $y = 35.4$ mm, followed by $y = 53.1$ mm, and $y = 70.8$ mm, and finally arriving at $y = 88.5$ mm. In the example of test P3, the Lüders band appears to move in the opposite direction, first arriving at $y = 88.5$ mm and at last at $y = 17.7$ mm. In other tests the band propagation is not continuous. For instance, for test P5, it is seen that the Lüders band arrives first at $y = 88.5$ mm, followed by $y = 70.8$ mm, then at $y = 17.7$ mm, followed by $y = 53.1$ mm, and finally at $y = 35.4$ mm. This indicates that there might be more than one Lüders band operating at the same time.

The temperature-time curves within the region of the Lüders band are shown in Figure 7, as obtained by DIT. The temperature histories for all coordinates indicated in Figure 2 are given. It is observed that the temperature decreases at all locations during straining in the elastic domain, owing to the thermoelastic effect, and stays constant until the arrival of the Lüders band. The temperature increases rapidly by about 0.5 K (0.5 °C) due to the plastic strain carried by the Lüders band, and then it stays constant again until the entire gage area of

the specimen has been covered by the Lüders band. The arrival times of the Lüders band are consistent with those obtained from the strain history in Figure 6, but some differences should be expected since the visual and thermal cameras monitored opposite faces of the specimen. The Lüders band reaches, for example, for test P5, first $y = 88.5$ mm, followed by $y = 70.8$ mm, then $y = 17.7$ mm and $y = 53.1$ mm almost simultaneously, and finally $y = 35.4$ mm. Again, the arrival times at the different locations indicate that the motion of the band is not continuous and that there could be two bands operating simultaneously.

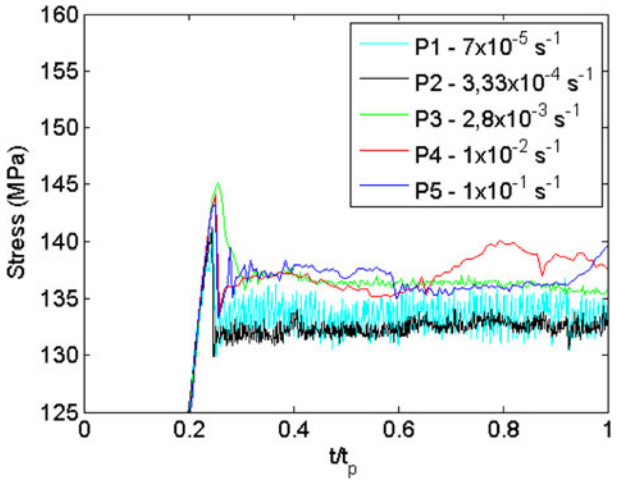

Fig. 5—Stress-time curves of tests P1, P2, P3, P4, and P5 in the Lüders plateau regime, where t_p is the duration of the Lüders plateau associated with each test.

Using DIC and DIT allows us to see more details of the nucleation and propagation of the Lüders and PLC bands. We present in the following these details for all tests carried out at an average strain rate range from 10^{-5} to 10^{-1} s^{-1}. Figure 8 displays the entire duration of the tests and shows the temperature change $\Delta T(x = 0,y,t)$ *vs* time along the longitudinal centerline of the specimen in the imaged area during the deformation process. The temperature change displayed in Figure 8 is obtained in the following way: at each acquisition time t, the acquired data are a matrix $T(x,y,t)$ representing the chart of temperatures as measured by the infrared camera. Here, (x,y) is a pixel from the imaged zone, where x and y represent lines (in the transverse direction) and columns (in the longitudinal direction corresponding to the tension axis) in the specimen, respectively. To minimize noise in the visualization of the bands, the average temperature change over a time increment $m\delta t$ is considered and expressed mathematically as

$$\Delta T(x,y,t) = \frac{1}{m}\sum_{j=0}^{j=m-1}\left[T(x,y,t+m\delta t) - T(x,y,t+j\delta t)\right] \quad [1]$$

where δt is the acquisition shutter (in time between individual frames). The choice of the parameter m

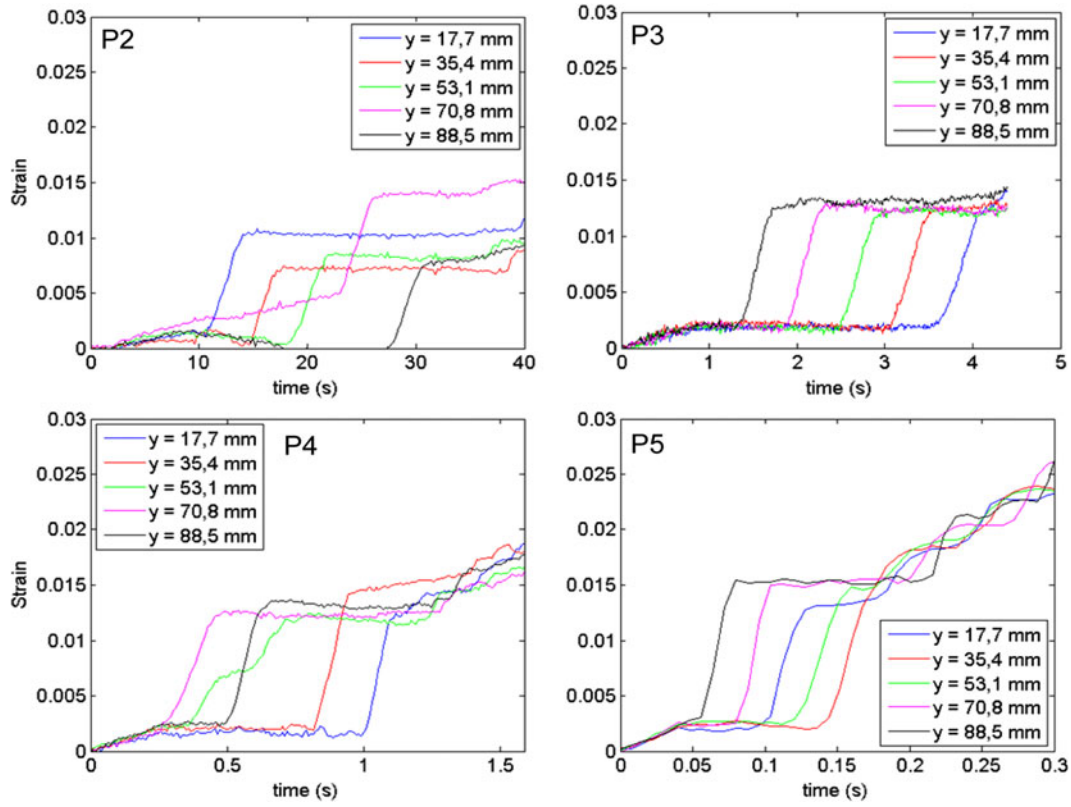

Fig. 6—Strain-time curves from tests P2, P3, P4 and P5 within the region of the Lüders plateau. The curves are given for five different locations in the gage section with reference to Fig. 2.

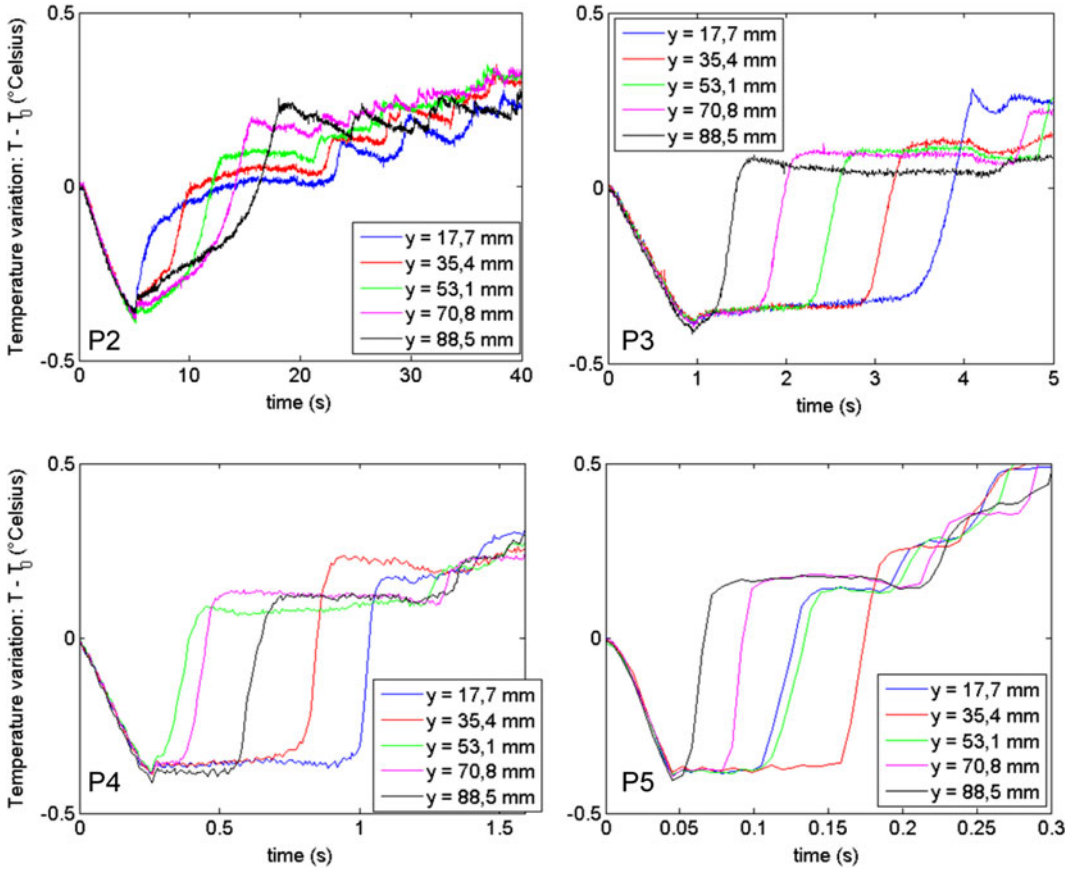

Fig. 7—Temperature-time curves from tests P2, P3, P4, and P5 within the region of the Lüders plateau. The curves are given for five different locations in the gage section with reference to Fig. 2.

depends on the crosshead velocity and the acquisition speed during the test. For the tests carried out in this work, $m = 50$ was used for P1 and P2, $m = 10$ was used for P3 and P4, and $m = 1$ was used for P5.

In Figure 8, the force-time curve is superimposed on the spatiotemporal temperature change $\Delta T(x = 0,y,t)$ to help in the interpretation, and the white vertical dashed line indicates the transition when the Lüders band disappears and PLC bands appear in the specimen. The same spatiotemporal representation during the Lüders plateau regime is given in Figure 9 in order to demonstrate more clearly the band behavior. It is clearly seen that two Lüders bands nucleate at $y \approx 30$ mm for test P2 and at $y \approx 60$ mm for test P4, while for test P5, they disappear at $y \approx 40$ mm. For test P3, there is only one Lüders band that propagates from the bottom to the top along the entire gage length of the specimen. For test P4, for example, the band that propagates in the positive direction of the y-axis is moving in a continuous manner. In contrast, the band moving in the other direction exhibits some discontinuities for y between 50 and 40 mm. The fact that two bands are operating at the same time is consistent with the findings presented in Figures 6 and 7. At the end of the Lüders plateau, PLC bands start to propagate across the gage section, as clearly seen from Figure 8. This spatiotemporal map confirms that sometimes more than one PLC band operate simultaneously. It is further observed that the band velocity decreases as the strain increases and the work-hardening decreases. At the same time, the temperature pulse, and therefore also the strain increment, induced by the band increases. Another observation is that the number of PLC bands up to necking decreases with increasing strain rate and that the intensity of the bands increases.

The band morphology is shown in Figure 10 for all tests. The spatial distribution of the strain increment from DIC and the temperature variation from DIT are compared in the figure. It is seen that the results are consistent with respect to the morphology of the PLC band. The symmetric orientation of the bands is explained by the fact that the images for DIC and DIT are of the two opposite faces of the specimen. The band width is estimated to be 5 mm, while the band orientation (defined as the angle between the band and the horizontal x-axis) is approximately 30 deg. Further, the figure confirms that two bands may operate at the same time, which is the case at time $t = 1.6$ seconds for test P5. Figure 11 provides a three-dimensional illustration of the morphology of the PLC bands at two different instants for test P5 in terms of the temperature-variation field.

Figure 12 shows the normalized strain and temperature *vs* time for tests P2, P3, P4, and P5, where $\varepsilon^* = \varepsilon/\varepsilon_{\max}$ is the normalized strain and $T^* = (T - T_{\min})/(T_{\max} - T_{\min})$ is the normalized temperature. Here, $\varepsilon_{\max}$

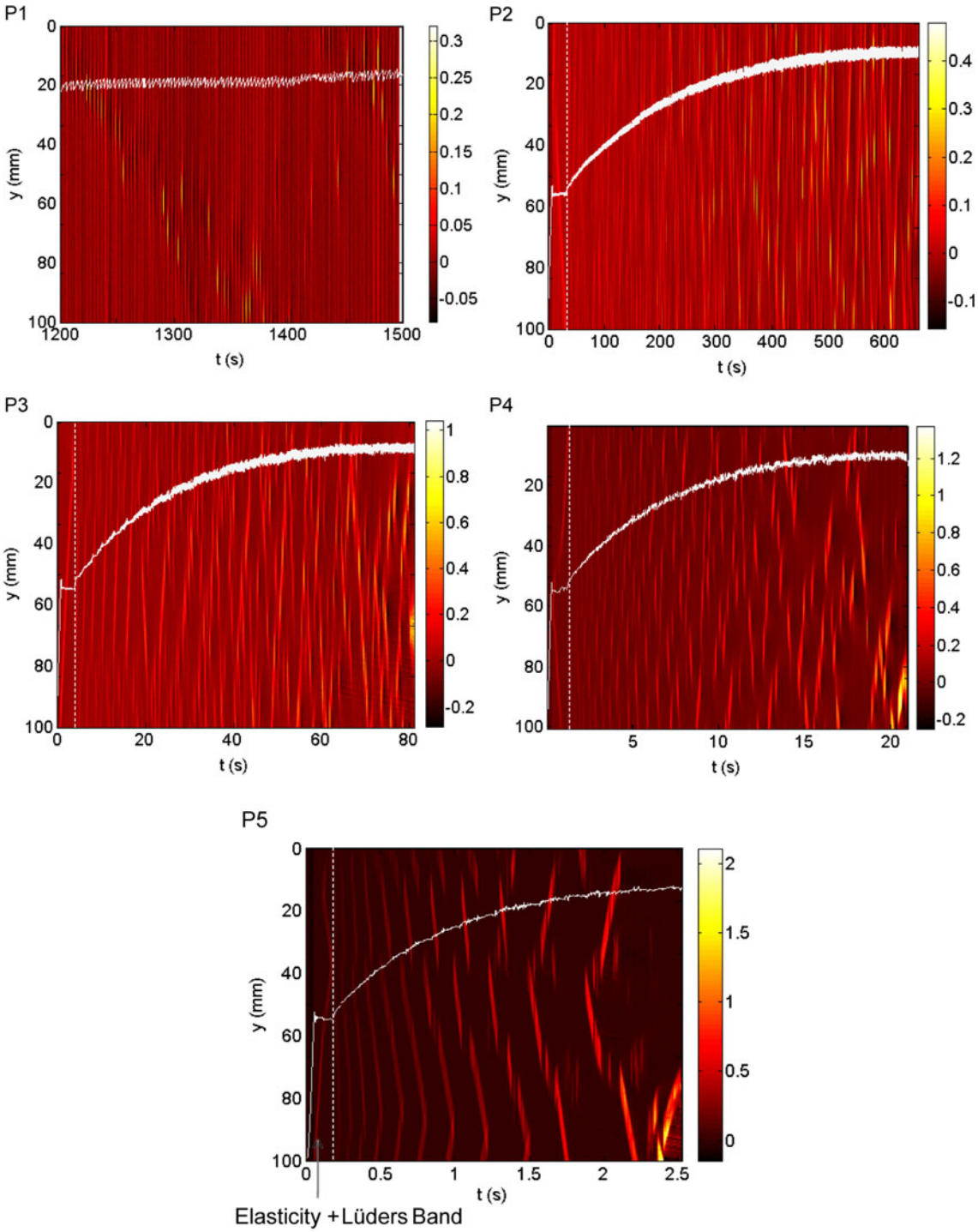

Fig. 8—Spatiotemporal temperature change as observed with DIT in tests P1, P2, P3, P4, and P5 with the force-time curve superimposed. The vertical white dashed line indicates the transition when the Lüders band disappears and PLC bands appear in the specimen.

is the strain at maximum force (*i.e.*, at incipient necking), T_{min} is the minimum temperature, and T_{max} is the temperature at maximum force. The data are acquired at the coordinate $y = 53.1$ mm. The staircase-like appearance of the strain-time curve is the signature of the PLC effect, since it indicates that the strain at a given location increases only during the time it takes the PLC band to pass by the optical gage. We further note that the strain carried by the band increases with time and, thus, with increasing strain. The temperature history has similar appearance to the strain history, and we see that the temperature increment increases with straining. This is consistent with the strain history data, and simply implies that the plastic work carried out during the passing of the band increases with strain. The figure further confirms that the PLC bands get more

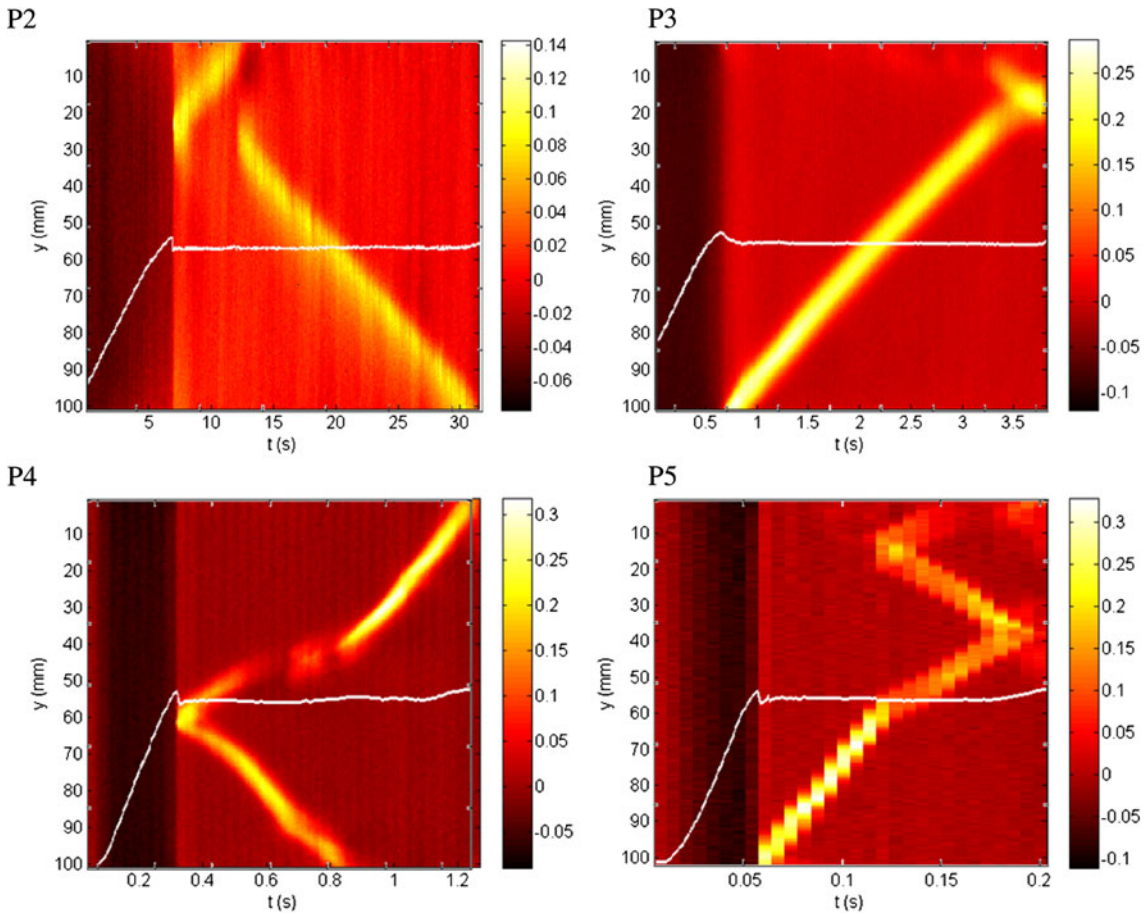

Fig. 9—Spatiotemporal temperature change during the Lüders plateau as observed with DIT in tests P2, P3, P4, and P5 with the force-time curve superimposed.

intense, in the sense that they carry more strain as the strain rate is increased. The encircled region of Figure 12 shows where the Lüders band appears and is followed by the PLC bands.

IV. DISCUSSION

A. *Yield Point, Lüders Plateau, and Serrated Yielding*

The material exhibits a sharp yield point at all strain rates tested. This is a result of the strain aging phenomenon, and the reason for the sharp yield point is pinning of dislocations by interaction with solutes that migrate to the dislocations during the aging time.[8] In this case, the aging time is the time from manufacturing of the sheet to the execution of the tensile tests. The Lüders band is then related to unlocking of dislocations in the case of weak pinning and formation of new dislocations in the case of strong pinning.[9] Similar observations for Al-Mg alloys were reported in several studies, *e.g.,* References 10 through 15. Robinson and Shaw[10] found that Lüdering occurred for an AA5182 alloy that was cold worked, annealed at 573 K (300 °C) for 30 minutes, and then air cooled. When the same alloy was cold rolled, annealed at 723 K (450 °C) for 10 minutes and water quenched, the Lüders extension was absent. The materials had similar grain sizes. Robinson and Shaw[10] suggest that the high uniform density of dislocations in the quenched material is sufficient to remove the yield point, and that the stronger static strain aging in the air-cooled material is due to the higher ratio of solute atoms to dislocation line length and the longer time available for solute migration in the period of the air cooling. Similar conclusions were also made by Rossig *et al.*[11] Lloyd *et al.*[12] studied the yield point elongation in the 5182-O alloy. They conclude that the occurrence of the Lüders effect was linked to the structure of the grain boundaries. Processing histories leading to grain boundaries free of defects resulted in the Lüders effect, whereas treatments giving a high density of grain boundary dislocations removed it. The result implies that segregation to individual dislocations and segregation to grain boundaries are both important processes. The room-temperature deformation behavior of an Al-Mg6.5 alloy sheet was investigated by Romhanji *et al.*[13] The material was cold rolled with reductions between 5 and 70 pct and then annealed at 593 K (320 °C) for 3 hours. The Lüders extension was suppressed for the materials with rolling reductions less than 15 to 20 pct. For these materials, the rolling and annealing resulted in well-defined subgrains of small size. The fine cell structure implies a high dislocation density and, thus, a more dilute solute atmosphere.

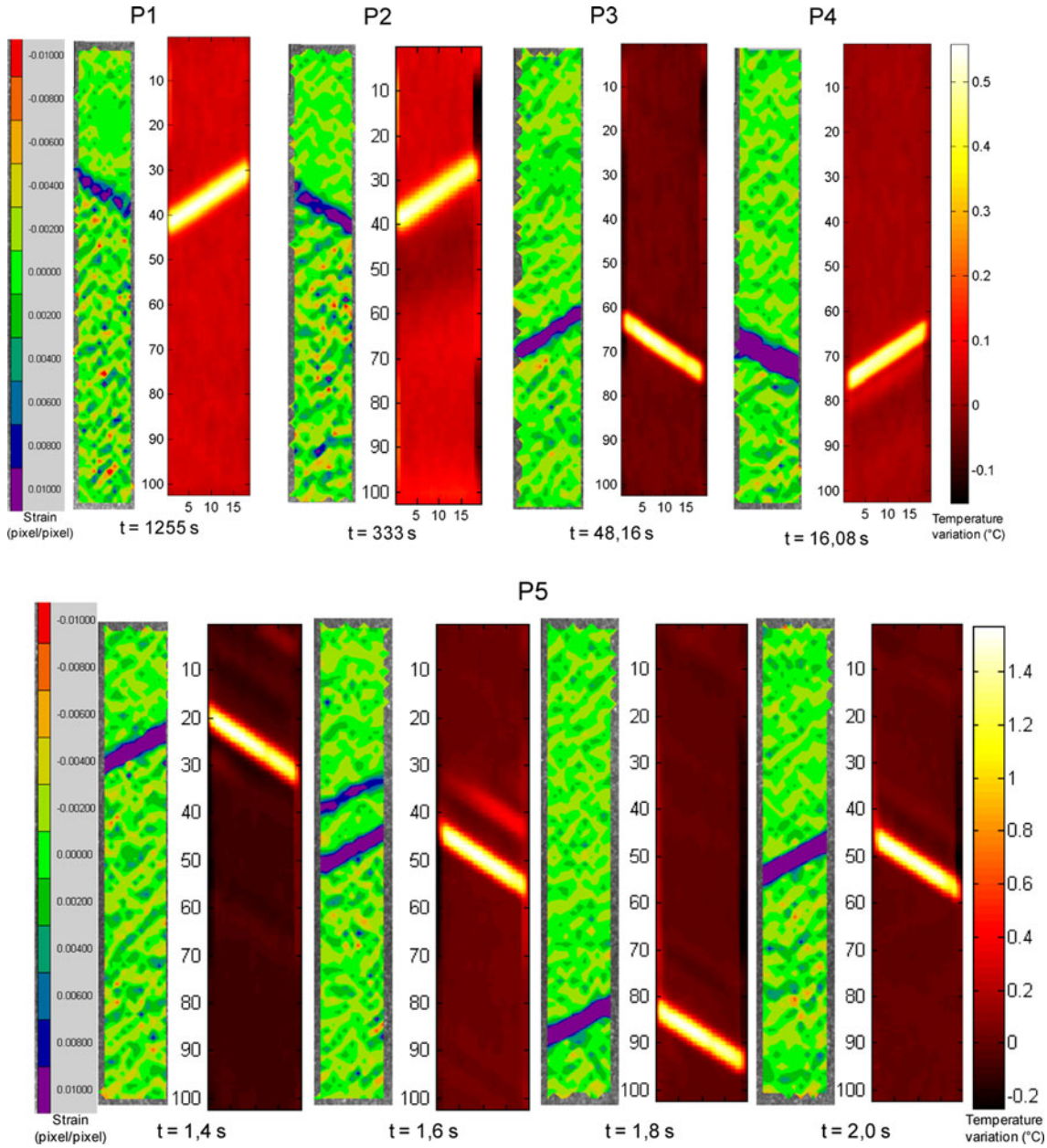

Fig. 10—Spatial distribution of strain variation from DIC (left) and temperature variation from DIT (right) at different times for tests P1, P2, P3, P4 (top), and P5 (bottom). Note that DIC and DIT images are taken on the two faces of the specimen, which explains the symmetric orientations of the band.

Higher rolling reductions led to a fully recrystallized microstructure with lower dislocation density after annealing. This leads to more favourable conditions for static strain aging, and for that reason, these materials exhibited Lüders extensions.

The yield point (upper yield stress) and the average flow stress within the Lüders plateau (lower yield stress) seem to be rather insensitive to the strain rate, and the difference between the upper and the lower yield stresses is about 10 MPa. Romhanji *et al.*[13] found that the yield stress (or rather the plateau stress) was practically insensitive to the strain rate for the fully recrystallized materials for which the Lüders extension occurred. From Figure 6, it is seen that the strain carried by the Lüders band is about 0.01 for the lowest strain rate and increases somewhat with the strain rate. The plastic work done as the Lüders band passes by a given location leads to a temperature increase of approximately 0.5 K (0.5 °C) (Figure 7). If we assume, for simplicity, that the thermomechanical process is adiabatic and that about 90 pct of the plastic work is dissipated as heat, the temperature increase ΔT is given as

$$\Delta T = 0.9 \frac{\bar{\sigma} \Delta \bar{\varepsilon}}{\rho C} \qquad [2]$$

where $\bar{\sigma}$ is the average flow stress within the Lüders plateau, $\Delta \bar{\varepsilon}$ is the plastic strain increment, ρ is the

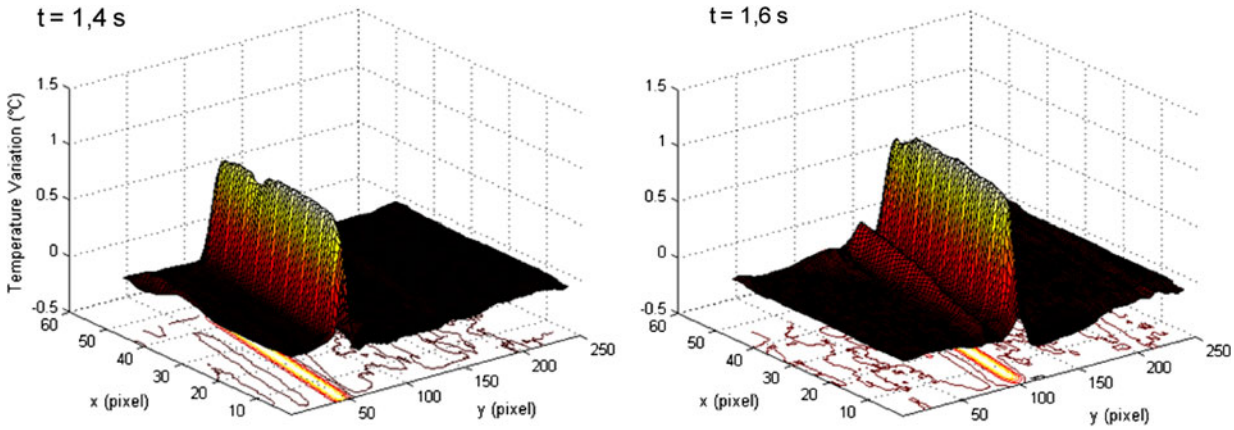

Fig. 11—Temperature variation field at $t = 1.4$ s (left) and $t = 1.6$ s for test P5 (also Fig. 9, bottom).

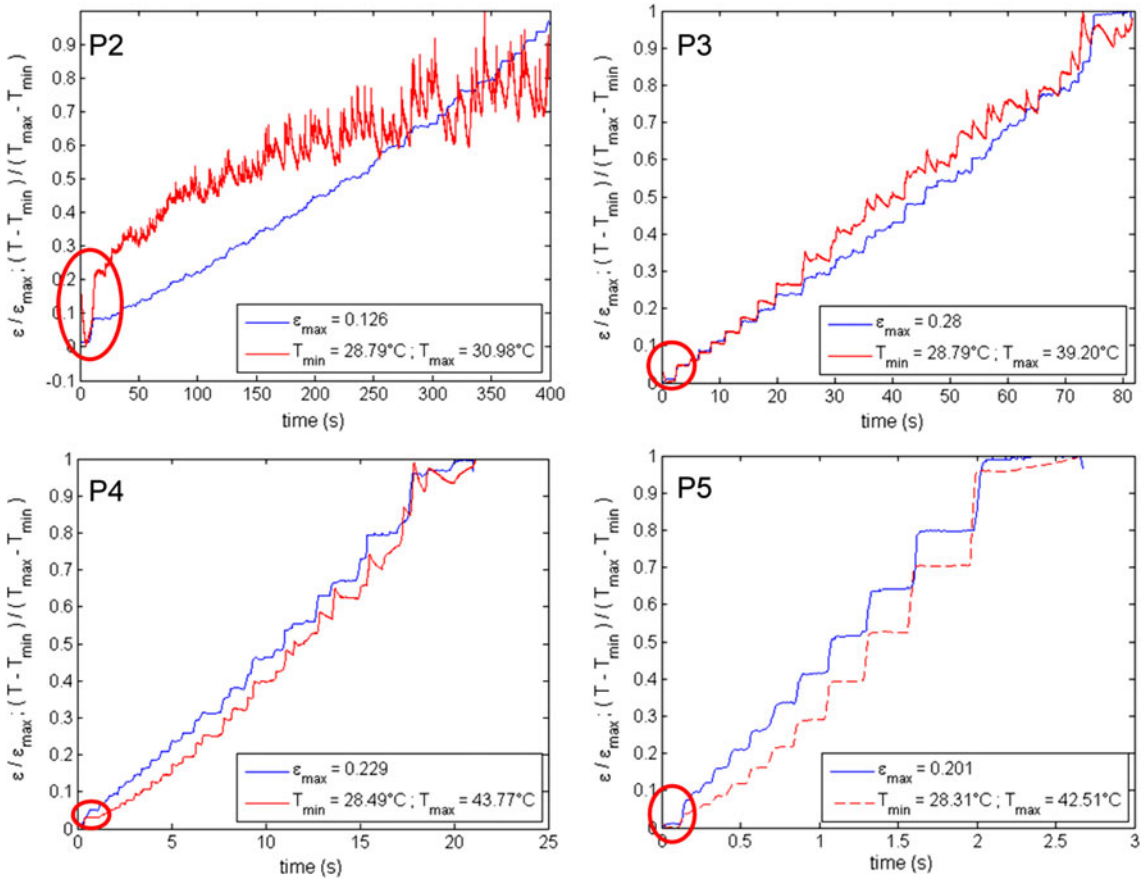

Fig. 12—Normalized strain and temperature *vs* time at coordinate $y = 53.1$ mm for tests P2, P3, P4, and P5. Note that the encircled region corresponds to the Lüders band.

density of the material, and C is the specific heat. From the experimental results, we have that $\bar{\sigma} \approx 135 \cdot 10^6 \text{N/m}^2$ and $\Delta\bar{\varepsilon} \approx 0.01$, while from MatWeb,[16] we find that $\rho \approx 2650$ kg/m^3 and $C \approx 904$ J/kg K for AA5182 in O temper. Using these data, we obtain $\Delta T \approx 0.5$ K (0.5 °C) from Eq. [2], which is certainly close to the value measured with DIT.

Another important observation is that jerky flow appears as soon as the material has entered into the Lüders plateau. The serrations indicate that there is no critical strain for the onset of the PLC effect; instead, it occurs at incipient yielding and seems to coexist with the Lüders band. Since this occurs in all tests, we conclude that the material exhibits negative steady-state SRS within the actual range of strain rates at room temperature and that the critical strain is zero. These findings are in agreement with the observations by Robinson and Shaw[10] and Picu *et al.*[14] for the same alloy. Another

explanation proposed by Ohtani and Inagaki[15] is that the Lüders strain exceeds the critical strain for the PLC effect to occur, and accordingly, serrated yielding will commence in a region right behind the front of the propagating Lüders band.

The amplitude of the serrations in the stress-time curve is strongest for the lowest strain rate and decreases as the strain rate is increased. Similar observations were reported by Kang *et al.*[17] for AA5754 (AlMg3) sheets. At the same time, the spatiotemporal map in Figure 8 indicates that the PLC bands get more intense for higher strain rates, in the sense that the strain increment produced by one passing of the band increases. The normalized strain-time curves at the center of the gage area presented in Figure 12 indicate that the band propagation becomes steadier as the strain rate increases. These curves also show that the strain increment produced by the PLC band (also denoted the band strain) increases markedly and the band velocity decreases as the work-hardening rate of the material decreases. Kang *et al.*[17] also found that the band strain increases with the global strain for AA5754.

B. *Work Hardening and Necking*

The force-elongation curves show that the work-hardening rate decreases with strain rate, while the flow stress on the yield plateau is less affected (Figure 3). Thus, it seems that the main effect of DSA is to increase the strength of the interaction between mobile and forest dislocations, as proposed by Mulford and Kocks[18] and later discussed by Wycliffe *et al.*[19] and van den Beukel and Kocks.[20] As discussed in Reference 20, the aging may possibly affect both the friction stress and the forest hardening. The observed reduction of the work-hardening rate is further in agreement with the more recent theories for DSA developed by Picu[21] and Soare and Curtin.[22] In particular, Picu[21] proposed a mechanism for DSA based on solute clustering at forest dislocations and its effect on the strength of dislocation junctions. Using a model constructed with this mechanism as its basis, Picu *et al.*[14] were able to capture several of the observed characteristics of the negative SRS of the AA5182 material in O temper and to describe the variation of the flow stress and hardening rate with temperature in the negative SRS region.

The elongation at ultimate force is determined by the onset of necking. The broken specimens hardly exhibited any evidence of diffuse necking, which indicates that local necking occurs almost immediately after reaching the maximum force. It is seen from the force-elongation curves in Figure 3 that the elongation at maximum force decreases with increasing strain rate. There seem to be two possible reasons for this observation. (1) The most obvious is the reduction of the work-hardening rate with increasing strain rate, which will tend to reduce the strain to necking, according to the Considère criterion. This tendency is at least partly counterbalanced by the lower flow stress, since the criterion states that necking occurs as the work-hardening rate equals flow stress. (2) Another explanation is that the PLC bands work as geometrical imperfections in the tensile specimen, owing to the local strain increment produced by the propagating band. This has been investigated by Kang *et al.*[17] The geometrical imperfection would result in lower strain to necking. Since the strain increment produced by the PLC bands seems to increase with increasing strain rate, it could be that this effect becomes more important as the deformation rate is increased.

C. *Comparison of Lüders Bands and PLC Bands*

One important observation in the behavior of AA5182 in O temper is the apparent existence of both Lüders and PLC bands. Besides, the plateau corresponding to the Lüders behavior is serrated. Furthermore, the serrations observed during the plateaus have exactly the same characteristics as the serrations observed for usual PLC bands. Their magnitudes increase when the strain rate is decreased; their shape also changes in a similar way when the strain rate is increased. The only difference is the presence of a yield point and that the average slope of the stress-strain curve is approximately zero as for the Lüders bands. Therefore, the observed bands share some properties from the classical PLC bands and others from Lüders bands. At first sight, the question arises whether the serrations are associated to secondary PLC bands superposed on a usual Lüders band or if this is some special type of bands. It is interesting to note that serrated Lüdering was also observed in steel.[23]

Usually, when comparing PLC bands to Lüders bands, major differences between the two types are observed: on the one hand, Lüders bands propagate only once in the specimen while PLC bands propagate repeatedly; on the other hand, the slope of the stress-strain curve is zero during the propagation of a Lüders band, while the slope of the overall stress-strain curve during the propagation of a PLC band is positive.

These differences were extensively studied by Wijler *et al.*,[24] who reported different types of deformation bands for a gold-copper alloy, namely, Au (14 at. pct Cu). Their reasoning was the following: during the propagation of the first PLC band, an almost uniform deformation rate is maintained in front of the band. Therefore, the band meets material, which was deformed to an increasing degree, and this requires an increasing stress for the band to propagate. The strain gradient met by the band is also enhanced by the passage of the band. Due to this strain gradient along the specimen, every fresh band will start at the end where the deformation is lowest. Following this, Wijler *et al.*[24] suggested that if one prevents the buildup of this strain gradient, then the shape of the stress-strain curve should be flat as in the case of a Lüders band. When the band has passed through the specimen, the strain is increased, and due to work hardening, the next band requires a stress jump. This was then experimentally verified. The strain gradient was suppressed by a homogeneous prestraining of the material at a high strain rate followed by sufficient aging in order to anchor the dislocations, after which the material was deformed at a relatively small strain rate for DSA to occur. Wijler *et al.*[24] also suggest that one can obtain a

similar situation with a gradient of aging rather than a strain gradient.

However, there are also some characteristic differences between the results obtained here for AA5182-O and those of Wijler *et al.*[24] The first one is related to the yield point. For our material, a usual yield point followed by the plateau is observed just like in a Lüders band if one disregards the serrations seen during the plateau. For the gold-copper alloy investigated by Wijler *et al.*,[24] a sharp yield point is observed, which is, however, immediately followed by a sharp increase of the flow stress above the yield point; and only after this is the serrated plateau observed (Figures 1 and 6 of Reference 24). The second one is that several plateaus were observed for the gold-copper alloy, each one followed by a stress jump and corresponding to a new band, while for AA5182-O, only one plateau is observed followed by normal PLC behavior. We note, however, that Wijler *et al.*[24] mention that they also observed situations where only one plateau was seen followed by normal PLC behavior, and this was attributed to the experimental conditions (prestrain, aging temperature, and aging time).

The nature of the strain gradients in the specimens of AA5182-O can be evaluated from the curves shown in Figure 6. Except for the test P2 (note that the same figure is not available for P1), in the three other tests, the plastic strain rate is almost zero outside the band. Hence, the strain gradient is negligible, leading to the plateau behavior.

V. CONCLUSIONS

Using tensile tests at different strain rates in combination with digital image correlation (DIC) and digital infrared thermography (DIT), the spatial and temporal characteristics of Lüders and Portevin–Le Chatelier bands in the Al-Mg alloy AA5182 in O temper were studied. The tests were performed at strain rates between 10^{-5} and 10^{-1} $s^{-1}$and at room temperature.

The material exhibited a sharp yield point, and Lüders band propagation was observed at all the strain rates. Jerky flow occurred all along the Lüders plateau and into the hardening region of the stress-strain curve. It thus seems that the material exhibits negative SRS at room temperature, and no critical strain is required for the onset of jerky flow. At the end of the Lüders plateau, Portevin–Le Chatelier bands immediately started to propagate across the gage length of the specimen. The work hardening of the material was found to diminish consistently with increasing strain rate, while the flow stress on the Lüders plateau was less affected by the strain rate. This indicates that the dynamic strain ageing mainly affects the strength of the interaction between mobile and forest dislocations. The strain to necking was found to decrease gradually with increasing strain rate, which is consistent with the lower work-hardening rate at the higher strain rates.

The combined use of DIC and DIT allowed a more precise investigation of the Lüders and PLC bands from the mechanical and thermal points of view. It provides, in particular, better measures of all the characteristics of the bands (the width, orientation, and velocity of the bands; the strain rate inside the bands; and the strain and temperature increments induced by the passing of the bands), and also their morphology. One particular observation was the correlation between the temperature increase and the strain increment caused by the Lüders and PLC bands and how the strain rate affects this correlation. In perspective, the thermal analysis allows for energetic considerations, which will facilitate enhanced modeling of static and DSA processes through dissipation analysis. The spatiotemporal analysis also gives direct insight into the fracture process following the DSA phenomenon.

ACKNOWLEDGMENTS

Two of the authors (JDE and OSH) acknowledge the award of a visiting professorship at LMT–Cachan. This work was supported by Ecole Normale Supérieure de Cachan, the French–Norwegian Foundation, and the Brazilian Ministry of Education through CAPES.

REFERENCES

1. A.H. Cottrell: *Phil. Mag.*, 1953, vol. 44, pp. 829–32.
2. A.H. Cottrell: *Dislocations and Plastic Flow in Crystals*, Oxford University Press, Oxford, United Kingdom, 1953.
3. L.P. Kubin and Y. Estrin: *Acta Metall.*, 1985, vol. 33, pp. 397–407.
4. P.G. McCormick: *Acta Metall.*, 1988, vol. 36, pp. 3061–67.
5. E. Rizzi and P. Hähner: *Int. J. Plast.*, 2004, vol. 20, pp. 121–65.
6. F. Hild and S. Roux: *Strain*, 2006, vol. 42, pp. 69–80.
7. G. Besnard, F. Hild, and S. Roux: *Exp. Mechan.*, 2006, vol. 46, pp. 789–803.
8. A.H. Cottrell and B.A. Bilby: *Proc. Phys. Soc. A*, 1949, vol. 62, pp. 49–62.
9. R.W.K. Honeycombe: *The Plastic Deformation of Metals*, 2nd ed., St Martin Press, New York, 1984.
10. J.M. Robinson and M.P Shaw: *Mater. Sci. Eng. A*, 1994, vol. 174, pp. 1–7.
11. H.H. Rossig, G. Ibe, and W. Gruhl: *Metallkunde*, 1974, vol. 28, pp. 232–37.
12. D.J. Lloyd, S.A. Court, and K.M. Gatenby: *Mater. Sci. Technol.*, 1997, vol. 13, pp. 660–66.
13. E. Romhanji, M. Popovic, and V. Radmilovic: *Z. Metallkd.*, 1999, vol. 90, pp. 305–10.
14. R.C. Picu, G. Vincze, F. Ozturk, J.J. Gracio, F. Barlat, and A.M. Maniatty: *Mater. Sci. Eng. A*, 2005, vol. 390, pp. 334–43.
15. S. Ohtani and H. Inagaki: *Mater. Sci. Forum,* 2002, vols. 396–402, pp. 1049–54.
16. MatWeb: *Material Property Data*, <http://www.matweb.com> [accessed 15.04.10].
17. J. Kang, D.S. Wilkinson, J.D. Embury, M. Jain, and A.J. Beaudoin: *Scripta Mater.*, 2005, vol. 53, pp. 499–503.
18. R.A. Mulford and U.F. Kocks: *Acta Metall.*, 1979, vol. 27, pp. 1125–34.
19. P. Wycliffe, U.F. Kocks, and J.D. Embury: *Scripta Metall.*, 1980, vol. 14, pp. 1349–54.
20. A. van den Beukel and U.F. Kocks: *Acta Metall.,* 1982, vol. 30, pp. 1027–34.
21. R.C. Picu: *Acta Mater.*, 2004, vol. 52, pp. 3447–58.
22. M.A. Soare and W.A. Curtin: *Acta Mater.*, 2008, vol. 56, pp. 4046–61.
23. J.S. Blakemore and E.O. Hall: *Iron Steel Inst.*, 1966, vol. 204, pp. 817–20.
24. A. Wijler, J. Schade van Westrum, and A. van den Beukel: *Acta Metall.*, 1972, vol. 20, pp. 355–62.